Available online at www.sciencedirect.com
ScienceDirect
Ceramics International 37 (2011) 1313–1319
CERAMICS INTERNATIONAL
www.elsevier.com/locate/ceramint

Synthesis, structural and magnetic properties of nanostructured $Ca_{0.9}Gd_{0.1}MnO_3$ obtained by modified glycine nitrate procedure (MGNP)

Milena Rosić [a,*], Mihovil Logar [b], Aleksandar Devečerski [a], Marija Prekajski [a], Ana Radosavljević-Mihajlović [a], Vladan Kusigerski [c], Vojislav Spasojević [c], Branko Matović [a]

[a] Laboratory for Material Science, Institute of Nuclear Sciences "Vinča", University of Belgrade, P.O. Box 522, 11001 Belgrade, Serbia
[b] Faculty of Mining and Geology, University of Belgrade, Djušina 7, 11000 Belgrade, Serbia
[c] Condensed Matter Physics Laboratory, Institute of Nuclear Sciences "Vinča", University of Belgrade, P.O. Box 522, 11001 Belgrade, Serbia

Received 29 September 2010; received in revised form 31 October 2010; accepted 11 December 2010
Available online 22 January 2011

Abstract

$Ca_{0.9}Gd_{0.1}MnO_3$ nanopowders with perovskite type crystal structure were synthesized by modified glycine nitrate procedure. Nanopowders were prepared by combining glycine with metal nitrates and/or metal acetates in their appropriate stoichiometric ratios. Modification of the procedure was performed by partial replacement of nitrates by acetates, in order to control the burn-up reaction. Obtained $Ca_{0.9}Gd_{0.1}MnO_3$ powders were calcinated in the temperature interval from 850 °C to 950 °C for 10 min. Properties such as phase evolution, lattice parameters, chemical composition and magnetic properties were monitored by DTA, X-ray diffraction, SEM/EDS and magnetic measurements. Magnetic measurements performed at the sample with the smallest crystallite size showed that a 10% of Gd^{3+} substituted Ca^{2+} ions changes antiferromagnetic properties of $CaMnO_3$ by the introduction of ferromagnetic interaction due to a double exchange between Mn^{3+} and Mn^{4+} ions. Presence of competing interactions and their randomness lead to a formation of a spin glass state below Neel temperature T_N = 110 K. From the high temperature magnetic susceptibility measurements effective magnetic moment of manganese ions is determined which lies between the values for Mn^{3+} and Mn^{4+} ions.

Keywords: Nanostructured materials; Spin glasses; Thermal analysis; Magnetic measurements

1. Introduction

Perovskite-type compounds have been attracting a large attention in a wide range of both practical and scientific interests due to a variety of their unique behaviour regarding ferroelectric, ferromagnetic, fast-ion conducting, and superconducting properties [1,2]. Many investigations on the substitution of rare earth ion in $ReMnO_3$ (Re = La, Nd, Gd, etc.) by Ca^{2+}, Sr^{2+} and Ba^{2+} have been conducted [3–7]. Transition metal-containing perovskites provide an important class of electronic and magnetic materials [8]. From the magnetic viewpoint, the nanoparticle manganites usually exhibit qualitatively new properties in respect to their bulk counterparts, such as changes in magnetic transition temperatures, the emergence of superparamagnetism, and size dependence of the saturation magnetization and coercivity [9–11].

Doped perovskite manganites have a general formula of $A_x^{2+}Re_{1-x}^{3+}Mn_x^{4+}Mn_{1-x}^{3+}O_x^{2-}$ (A: alkali earth element; Re: rare earth element). In Re-doped manganites, Mn can exist as Mn^{3+} and Mn^{4+} in order to maintain the charge neutrality of the compound. The dopant will either occupy the A site, the B site, or both of them (amphoteric) of the perovskite structure, depending on the Re radius. Typically, the larger Re atoms will occupy A sites, while the smaller cations prefer the B sites [12]. However in case of Gd, it will occupy A sites, because Gd^{3+} ions are much bigger than Mn cations. In addition, substituting of Mn for Gd will influence the change of manganese valence. The structure of manganites is governed by the Goldschmidts tolerance factor $f = (r_A + r_O)/\sqrt{2}\,(r_B + r_O)$ [13]. It measures the strain in the structure resulting from mismatch between the equilibrium A–O and B–O bond lengths. A Goldschmidts

* Corresponding author. Tel.: +381 11 3408 224; fax: +381 11 3408 224.
E-mail address: mrosic@vinca.rs (M. Rosić).

0272-8842/$36.00
doi:10.1016/j.ceramint.2010.12.015

tolerance factor $f = 1$ characterizes an unstrained cubic lattice while $f > 1$ and $f < 1$ represent a strain that is typically relaxed by distortion of the structure away from its ideal cubic form. Such distortion often takes the form of rigid rotation of MnO_6 octahedra, which changes the coordination sphere of A-site cation [13]. Goldschmidts tolerance factor is 1.00396, which leads us to the conclusion that the observed nanometric structure could be stable.

In spite of many already explored different perovskites, to our best knowledge there are no data in the literature about nanostructure $CaMnO_3$ doped with low amount of Gd. Several papers [14–17], have been published on polycrystalline $Ca_{1-x}Gd_xMnO_3$ where its structure, electrical and magnetic properties have been investigated in detail. However, all these works are not related to $Ca_{0.9}Gd_{0.1}MnO_3$ nanopowders and getting used to these long-term methods and overcome. Nanostructured $Ca_{1-x}Gd_xMnO_3$ obtained by cheap and quick method, like glycine nitrate procedure, can be relevant for the research in the field.

In undoped $CaMnO_3$, magnetic moments of Mn^{4+} ions are arranged antiferromagnetically, while by Gd^{3+} doping (electron doping) certain amount of Mn^{3+} ions emerges. Since interaction between Mn^{4+} and Mn^{3+} ions is ferromagnetic (double exchange), a certain degree of magnetic moments frustration is possible. Main goal of this work is to investigate the possibility to form nanostructure solid solutions with nominal compositions $Ca_{0.9}Gd_{0.1}MnO_3$ using a modified glycine nitrate procedure (MGNP) [18], and to analyse its structural properties and magnetic behaviour.

2. Experimental

The present trend in synthesis of new materials is to avoid brute force methods in order to have a better control of stoichiometry, structure and phase purity of metal oxides. Starting chemicals used for the synthesis of powders were aminoacteic acid–glycine (Fischer Scientific, USA), metallic acetate Mn ($Mn(CH_3CO_2)_2{\cdot}4H_2O$), and nitrates Mn, Ca, Gd ($Mn(NO_3)_2{\cdot}H_2O$, $Ca(NO_3)_2{\cdot}4H_2O$, $Gd(NO_3)_3{\cdot}6H_2O$), produced by Aldrich, USA. The compositions of reacting mixtures were calculated in two ways according to the nominal composition of the final reaction product as well as different precursors used. In first experimental set up, glycine was added into the mixed nitrate solution in a molar ratio of 1:1 for fuel:oxidant. In the second case, for stoichiometric combustion reaction, the amount of fuel is fixed on the basis of the principle of propellant chemistry [19]. According to the principle of propellant chemistry, for a stoichiometric redox reaction between a fuel and oxidizer, the ratio of net oxidizing valency of metal nitrate to net reducing valency of fuel should be unity. By convention, the valencies of carbon, nitrogen, oxygen, hydrogen, gadolinium, calcium and manganese are set as 4+, 0, 2−, 1+, 3+, 2+, and 2+, respectively. Using the valencies of these individual elements, the net oxidizing valency of $Gd(NO_3)_3$, $Ca(NO_3)_2$, $Mn(NO_3)_2$, and $Mn(CH_3CO_2)_2$ works out to be 15−, 10−, 10−, and 16 + , respectively, whereas the reducing valency of glycine works out to be 9+. Hence, for producing one mole of $Ca_{0.9}Gd_{0.1}MnO_3$ through the stochiometric reaction, for the first reaction 0.83 moles of glycine is required, for the second reaction 0.61 moles of glycine and for the third reaction 2.28 moles of glycine is required. Preparation of $Ca_{0.9}Gd_{0.1}MnO_3$ powders was performed according to reactions:

$$C_2H_5NO_2 + 0.5Mn(CH_3CO_2)_2{\cdot}4H_2O + 0.9Ca(NO_3)_2{\cdot}4H_2O + 0.5Mn(NO_3)_2{\cdot}H_2O + 0.1Gd(NO_3)_3{\cdot}6H_2O + 0.95O_2 \rightarrow Ca_{0.9}Gd_{0.1}MnO_3 + 2CH_3COOH + 4.1NO_2\uparrow + 6.7H_2O \quad (1)$$

$$C_2H_5NO_2 + Mn(CH_3CO_2)_2{\cdot}4H_2O + 0.9Ca(NO_3)_2{\cdot}4H_2O + 0.1Gd(NO_3)_3{\cdot}6H_2O + 1.2O_2 \rightarrow Ca_{0.9}Gd_{0.1}MnO_3 + 3CH_3COOH + 3.1NO_2\uparrow + 7.7H_2O \quad (2)$$

$$C_2H_5NO_2 + Mn(NO_3)_2{\cdot}H_2O + 0.9Ca(NO_3)_2{\cdot}4H_2O + 0.1Gd(NO_3)_3{\cdot}6H_2O + 0.7O_2 \rightarrow Ca_{0.9}Gd_{0.1}MnO_3 + CH_3COOH + 5.1NO_2\uparrow + 5.7H_2O \quad (3)$$

On the basis of two ways of calculations and three reaction models presented by Eqs. (1)–(3), six different samples were obtained.

Synthesis was carried out in a stainless steel reactor in which all reactants dissolved in distilled water were added according to the previously calculated composition of the final powder. Hence, when dissolved in water, initially it forms a heterogeneous medium where the reaction takes place at the interface [20].

The modernized furnace, Chevenard Joimer Instrument A.D.A.M.E.L. [21] equipped with Pt–PtRh thermocouples together with the digital data acquisition computer system has been used to obtain the DTA (differential thermal analysis). The t and Δt voltages were collected over the 16-bit USB-2523 AD converter with 1 Hz sampling rate. The heating rate was 8 °C/min. Consequently in the temperature range of 20–1000 °C around 7350 points were read. The reference material used was α-Al_2O_3. Simultaneous DTA of each reaction was carried out to study the decomposition behaviour and nature of the combustion reaction. On the basis of DTA analysis it is found that the resulting amorphous powders crystallize in the temperature range from 880 °C to 955 °C. In this manner, it was established calcination temperature (Nabertherm furnaces). The yield of powders was very close to the theoretically calculated ones, 96–99%.

Powder XRD patterns of all the powders were recorded on Simens X-ray diffractometer (Kristaloflex 500) with Ni filtered Cu K_α radiation and using Si as an external standard. The measurements were performed in the range 10–80° 2θ in a continuous scan mode with a step width of 0.02° and 0.5 s/step. The obtained data were fitted using peak-fitting program. The Lorentizian function gave the best fit to the experimental data.

Lattice parameters were refined from the fitted data using the least square procedure. Rietveld refinement is also done for the obtained sample with smaller crystallite size. The structure of obtained powder was determinate by X-ray powder diffraction on a Siemens D-500 XRPD diffractometar with Cu $K_{\alpha 1,2}$ radiation, at room temperature. Data for structural refinement were taken in the 2θ range 10–104.56°, with the step of 0.03° and scanning time of 14 s per step. The refinement was performed with the FullProf computer program [22–24] which adopts the Rietveld calculation method. The TCH pseudo-Voigt profile function was used.

Magnetic properties were measured by the Quantum Design SQUID magnetometer MPMS XL-5. Temperature dependence of magnetization $M(T)$ was measured in both zero-field cooled (ZFC) and field cooled (FC) regime, in two different magnetic fields of 100 Oe and 1000 Oe. Magnetization dependence on magnetic field strength $M(H)$ was measured at temperatures below and above phase transition temperatures. AC magnetic susceptibility was recorded at two frequencies (10 and 1000 Hz), with 4 Oe driving amplitude, in the temperature range encompassing spin-glass (SG) and antiferromagnetic–paramagnetic (AF–P) phase transitions.

3. Results and discussion

3.1. DTA

Fig. 1 shows the DTA curves for the synthesized powder of $Ca_{0.9}Gd_{0.1}MnO_3$. The thermal decompositions are described by the existence of three main degradation stages (endotherm, exotherm and endotherm, respectively). As shown in Fig. 1 the first one, starts from 84 °C to 210 °C corresponding to the elimination of absorbed water in the powder. This decomposition stage consists in an initial very weak endothermic effect (∼140 °C, shoulder) representing water evolving, followed by a fast and intensive exothermic process (second stage), consisting in simultaneous evolving of NO_3^- and glycine. Simultaneously, glycine is oxidized by nitrate anions [25]. Sharp exothermic peaks were found in two cases (curves a and b in Fig. 1), which indicate the occurrence of combustion reaction. The exothermal peaks at 206 °C and 285 °C indicate the decomposition and decarbonisation of the residue organic compounds in the powder, respectively [26]. Therefore, the second decomposition stage, accompanied by a medium exothermic effect, represents the burn up of the remainder carbonaceous residue. Third stage consists in an initial weak endothermic effect (∼910 °C) representing onset crystallize him.

Based on the DTA results the powders prepared by glycine route have been calcined at temperature range from 880 to 955 °C for 10 min. The results indicate that intimate mixing on the atomic level of the oxidant and the fuel in the form of a stable gel is necessary for the propagation of combustion reaction.

3.2. Powder XRD

XRD patterns of the powders obtained after combustion reaction (not shown) were found to be amorphous in nature, probably due to insufficient heat/temperature generated.

XRD diagrams of the $Ca_{0.9}Gd_{0.1}MnO_3$ powder after calcinations are shown in Fig. 2. All peaks are broad and with low intensities indicating nano-crystalline nature of the powders. The crystallite size has been calculated from FWHM (full width at half maximum) data using Scherrer formula [27]:

$$D = \frac{0.9\lambda}{\beta \cos\theta} \quad (4)$$

where D is the crystallite size in nm, λ is the radiation wavelength (0.154056 nm in present case, Cu target), 2θ is the diffraction angle, and β is the corrected line width at half peak intensity.

The crystallite size calculated on the basis of XRD data is shown in Table 1. It was found that all the samples obtained in

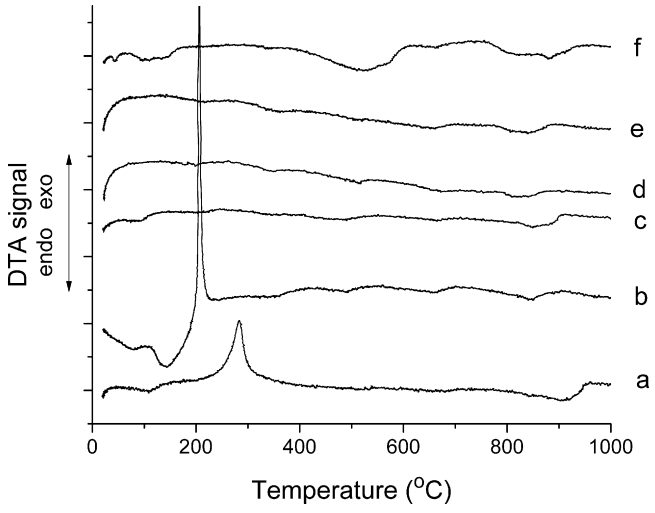

Fig. 1. DTA diagrams of synthesized $Ca_{0.9}Gd_{0.1}MnO_3$ obtained by MGNP method. Letters from a to f denote samples obtained from different precursors (see Table 1).

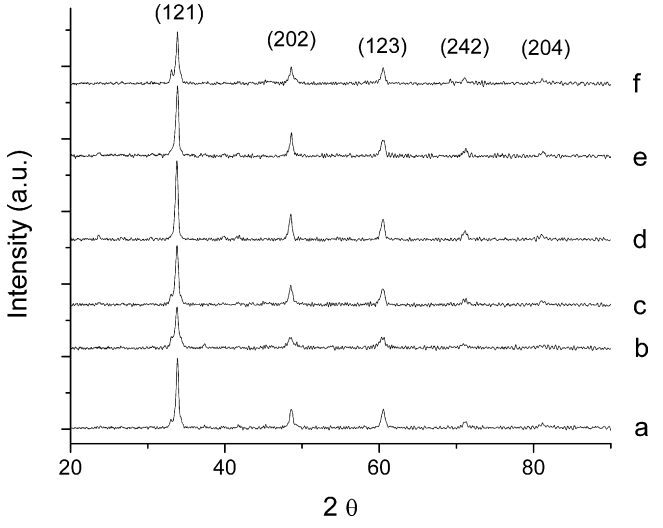

Fig. 2. XRD patterns of $Ca_{0.9}Gd_{0.1}MnO_3$ powder sample obtained by combustion synthesis. Letters from a to f denote samples obtained from different precursors (see Table 1).

Table 1
Crystallite size in relation to the methods and different precursors applied.

Method	Samples	Different precursors	Crystallite size (nm)
Nominal composition	a	$Mn(CH_3CO_2)_2{\cdot}4H_2O$ $Mn(NO_3)_2{\cdot}H_2O$ $Ca(NO_3)_2{\cdot}4H_2O$ $Gd(NO_3)_3{\cdot}6H_2O$	22
	d	$Mn(CH_3CO_2)_2{\cdot}4H_2O$ $Ca(NO_3)_2{\cdot}4H_2O$ $Gd(NO_3)_3{\cdot}6H_2O$	20
	f	$Mn(NO_3)_2{\cdot}H_2O$ $Ca(NO_3)_2{\cdot}4H_2O$ $Gd(NO_3)_3{\cdot}6H_2O$	22
Propellant chemistry	c	$Mn(CH_3CO_2)_2{\cdot}4H_2O$ $Mn(NO_3)_2{\cdot}H_2O$ $Ca(NO_3)_2{\cdot}4H_2O$ $Gd(NO_3)_3{\cdot}6H_2O$	17
	e	$Mn(CH_3CO_2)_2{\cdot}4H_2O$ $Ca(NO_3)_2{\cdot}4H_2O$ $Gd(NO_3)_3{\cdot}6H_2O$	19
	b	$Mn(NO_3)_2{\cdot}H_2O$ $Ca(NO_3)_2{\cdot}4H_2O$ $Gd(NO_3)_3{\cdot}6H_2O$	18

this work are nanocrystalites with the sizes ranging between 17 and 20 nm.

Samples d and e prepared without $Mn(NO_3)_2{\cdot}H_2O$, exhibit sharp diffraction lines, but we choose sample c for Rietveld analysis and magnetic measurements due to its smallest crystallite size.

The best fits between calculated and observed X-ray diffraction patterns for $Ca_{0.9}Gd_{0.1}MnO_3$ c sample are given in Fig. 3. All allowed Bragg reflections are shown by vertical bars. By inspecting difference between the experimental and calculated profiles, good agreement can be observed.

The crystal structure refinement was performed using the XRD data collected at room temperature by utilizing the FullProf program. The structure was described in the orthorhombic space group *Pnma* (No. 62) with (Ca, Gd) atoms located at *4c* positions, Mn atoms at *4b*, and oxygen atoms at *4c* and *8d* positions. The results of Rietveld refinement clearly demonstrated that in the case of Gd doped solid solutions the cations occupied A site. The obtained values of lattice parameters for $Ca_{0.9}Gd_{0.1}MnO_3$ are as follows: $a = 5.291(4)$, $b = 7.467(7)$, $c = 5.303(9)$, $V = 209.585$ Å and together with the ratio of Ca:Gd = 0.9:0.1, are very close to the nominal composition. Calculated unit cell volume of $Ca_{0.9}Gd_{0.1}MnO_3$ is higher than in Ref. [28] where it is 207.37(2) Å. The data from Ref. [28] were used as the starting model for refinement that indicated the presence of dopants in the structure. Occupation factor refinement shows that Ca shares the position with Gd (9.6%). This dopant causes the reduction of Mn^{4+} into Mn^{3+} and the increase of unit cell volume. Calculated value for $\langle Mn–O \rangle$ distance is 1.919 Å, and reason for this increase is the presence of Gd^{3+} and Mn^{3+} in the structure.

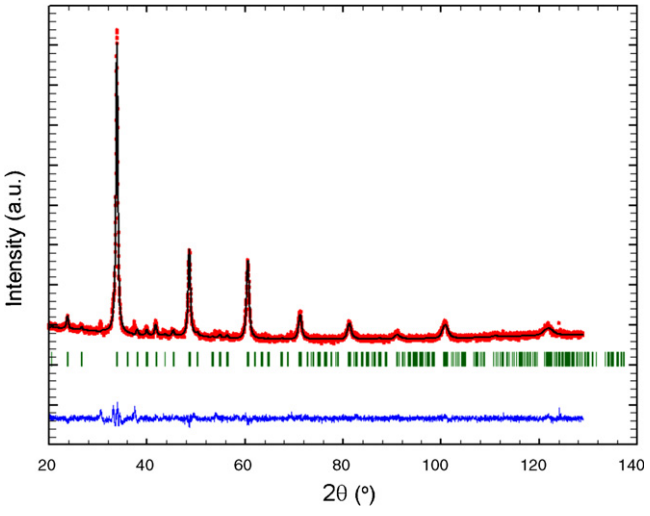

Fig. 3. Results of Rietveld refinement of the $Ca_{0.9}Gd_{0.1}MnO_3$ sample, calcined at 910 °C for 10 min. The positions of the Bragg reflections are indicated by vertical bars. The difference curve between the experimental and the calculated intensities is shown in the lower part of the diagram.

3.3. SEM

SEM investigation shows that all obtained powders have high tendency of agglomeration. Typical SEM image (Fig. 3) of the sample c showed that the powder has sponge morphology with large numbers of pores and voids. This porosity can be attributed to the large amount of gases escaping out of the reaction mixture during the combustion. During ignition, the heat dissipation and the evolution of gaseous products are taking place at various rates which ultimately lead to a localized heating and formation of large agglomerates. The porous nature is formed out of the fast expulsion of the gases. The chemical compositions can be clearly identified by the EDS analysis spectrum, which is also shown as an insert along with the SEM image. It confirms that the elemental composition is Ca, Gd, Mn and O, respectively and the powder has no other impurities (Fig. 4).

3.4. Magnetic properties

Temperature dependence of magnetization, recorded from 5 K up to 300 K, in two different magnetic fields is depicted in Fig. 5. The ZFC branch shows very slow increase of magnetization when temperature decreases from 300 K to about 130 K, and then an abrupt increase of magnetization is appreciable. This increase can be assigned to AF–P phase transition which is characteristic for manganites where Ca^{2+} molar fraction $x > 0.5$ [29,30]. Neel temperature $T_N = 110$ K, which is independent on magnetic field, was determined from dM/dT derivate (Fig. 5, inset b). Below T_N prominent bifurcation between ZFC and FC branches (empty and full symbols, respectively) is noticeable.

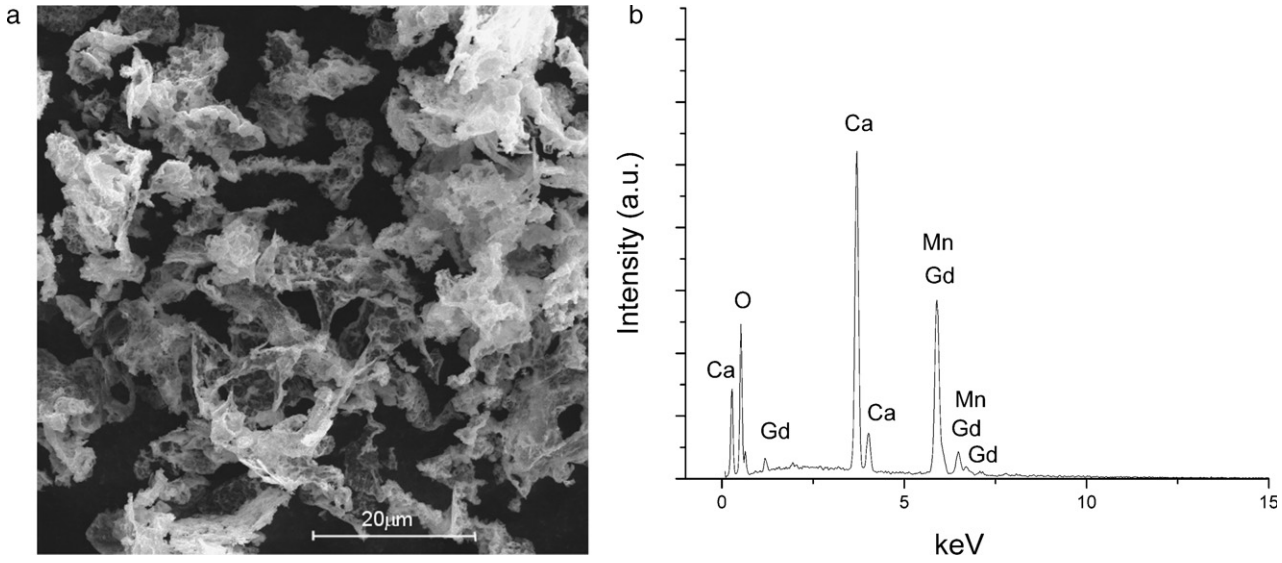

Fig. 4. SEM micrographs of $Ca_{0.9}Gd_{0.1}MnO_3$ powder and pattern from EDS X-ray detector.

FC branches for both applied magnetic fields continually increase, and for $H = 100$ Oe it shows plateau while for 1000 Oe at low temperature additional increase can be observed. This magnetization increase below T_N accompanied with plateau at low temperatures is characteristic of ferromagnetic. It is widely accepted that FM component in mixed valence manganite arises from double exchange interactions between Mn^{3+} and Mn^{4+} ions [1]. Since in ''pure'' $CaMnO_3$ only Mn^{4+} ions are present, Mn^{3+} ions appear after Gd^{3+} doping (electron doping), in order to preserve electroneutrality. Gd^{3+} ions replace Ca^{2+} at A site position, but their fraction is too low to establish long range magnetic order. Instead of this, due to Mn^{3+}–Mn^{4+} exchange interactions, short range ordering occurs, forming FM clusters in AF matrix. FM ordering in the clusters and AF interaction of the background cause the emergence of magnetic frustration that occurred in this system.

ZFC magnetization branches display more complex behaviour. Below T_N decrease of magnetization which is typical of AF transitions occurs but at lower temperatures additional maximum can be noticed (Fig. 5, inset a). Position and shape of this maximum depend on the magnetic field strength H in a way that it shifts to lower temperatures and becomes less pronounce in higher magnetic fields. This behaviour is typical of spin-glasses, and it occurs always when some kind of frustration of magnetic interactions is present. In addition, an increase of magnetization that is visible in both ZFC and FC branches for $T < 10$ K can be assign to the large contribution of Gd^{3+} paramagnetic moments ($\mu_{Gd^{3+}} = 7.94\mu_B$ [32]) which is particularly pronounced at low temperatures.

Further evidence of the spin-glass transition at low temperature gives AC susceptibility measurements recorded for two different field frequencies (Fig. 6). It is visible that position of peak (denoted by arrow) is shifted to the higher

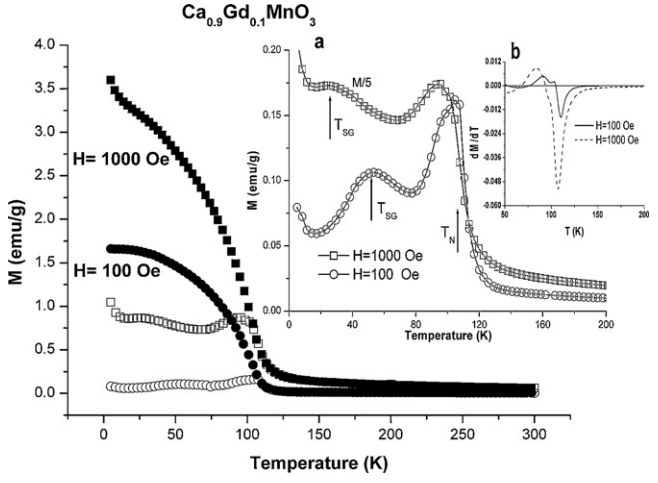

Fig. 5. Temperature dependence of ZFC (open symbols) and FC magnetization (full symbols) of $Gd_{0.1}Ca_{0.9}MnO_3$ in different magnetic fields. Inset a: Details of ZFC magnetization; spin-glass transitions are denoted by arrows; magnetization recorded in 1000 Oe is divided by 5. Inset b: dM/dT derivate vs. T encompassing AF–P transition.

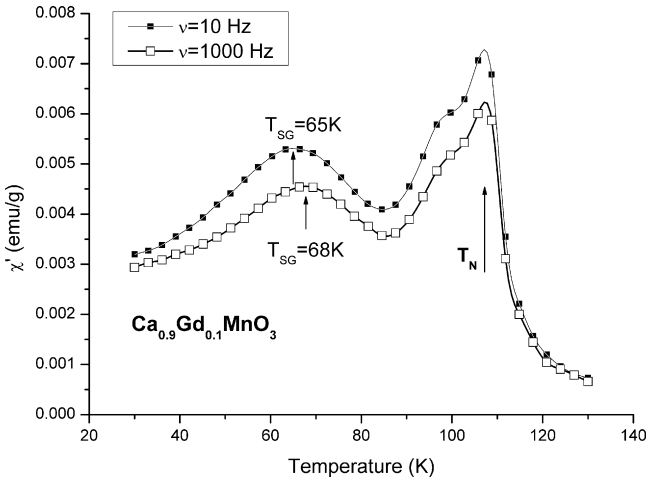

Fig. 6. Real part of AC susceptibility vs. temperature for two different frequencies.

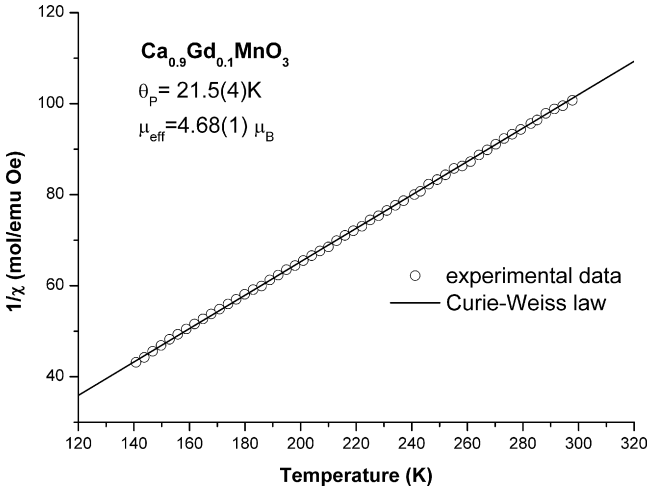

Fig. 7. High temperature dependence of inverse susceptibility recorded in $H = 100$ Oe for $T > 140$ K.

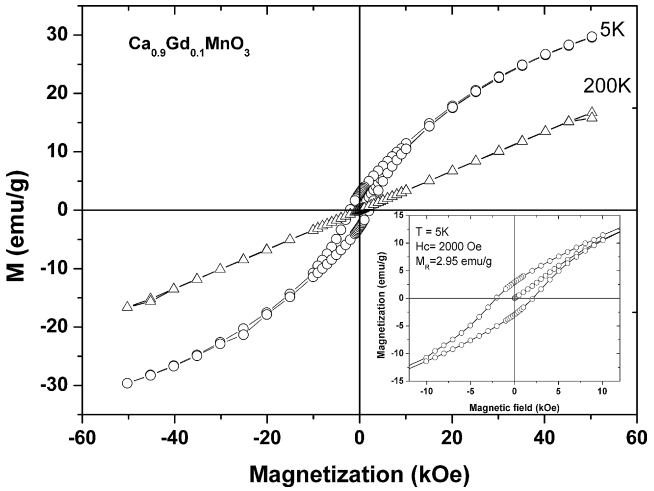

Fig. 8. Hysteresis loop of $Gd_{0.1}Ca_{0.9}MnO_3$ recorded at 5 K. Inset: Detail of $M(H)$ dependence.

temperature for higher frequency. It is a signature of a spin-glass behaviour [33], while AF–P phase transition denoted with T_N is not frequency dependant (see Fig. 6).

Temperature dependence of high temperature magnetic susceptibility was measured in the 140–300 K range and the applied field of 100 Oe. Inverse magnetic susceptibility (open symbols) vs. temperature is depicted in Fig. 7, as well as a fit of the experimental data to a Curie–Weiss law (solid line). It can be seen that in this temperature range Curie–Weiss law is fulfilled, and from this fit both effective magnetic moment $\mu_{eff} = (4.68 \pm 0.01)\mu_B$ and Curie–Weiss temperature $\theta_P = (21.5 \pm 0.4)$ K are determined. Positive value of Curie–Weiss temperature speaks in favour of a presence of weak ferromagnetic interaction among manganese ions. Similar result has been obtained for $Ca_{1-x}Nd_xMnO_3$ [31], where negative θ_P changes sign to positive for $0.05 \leq x \leq 0.1$, while for higher doping level, negative θ_P value is resumed. It is assumed that for this doping region ferromagnetic correlations are induced causing magnetic phase separation in which ferromagnetic components are embedded in antiferromagnetic matrix. Obtained μ_{eff} value includes contribution of both manganese and gadolinium ions. Thus, the contributions of Mn ions $\mu_{Mn^{3+,4+}}$ to the effective magnetic moment can be calculated from:

$$\mu^2_{Mn^{3+,4+}} = \mu^2_{eff} - 0.1 \times \mu^2_{Gd}, \quad (5)$$

where μ_{eff} is experimentally obtained overall effective magnetic moment ($4.68\mu_B$) while μ_{Gd} denotes gadolinium contribution ($\mu_{Gd^{3+}} = 7.94\mu_B$ [32]). The obtained manganese magnetic moment of $\mu_{Mn^{3+,4+}} = 3.96\mu_B$ is between the spin-only values for Mn^{3+} ($4.90\mu_B$) and Mn^{4+} ($3.87\mu_B$). If we write chemical formula for this compound as $Ca_{0.9}Gd_{0.1}Mn^{3+}{}_{1-x}Mn^{4+}{}_xO_3$ then contributions of both Mn ions with different valence states to the μ_{eff} can be estimated from:

$$\mu^2_{Mn^{3+,4+}} = x\mu^2_{Mn^{3+}} + (1-x)\mu^2_{Mn^{4+}}. \quad (6)$$

The value of $x = 0.08$ obtained from the expression (6) shows that Mn^{4+}/Mn^{3+} ratio is close to Ca^{2+}/Gd^{3+} ratio. This points to a good stochiometry with the small excess of oxygen of $\delta = 0.02$ that is within the experimental error.

$M(H)$ curves recorded at two temperatures are displayed in the Fig. 7. In the inset (bottom) details of $M(H)$ at $T = 5$ K are presented. It can be seen that for $T = 5$ K magnetization does not saturate even for 50 kOe due to the existence of antiferromagnetic interactions. Large coercivity ($H_C = 2000$ Oe) and remanence magnetization of $M_R = 2.95$ emu/g confirm our presupposition derived from FC measurements about existence of ferromagnetic ordered clusters at low temperature. At temperature $T = 200$ K, which is above T_N, sample is in a paramagnetic state (Fig. 8).

4. Conclusions

$Gd_{0.1}Ca_{0.9}MnO_3$ nanopowders were prepared by a modified glycine nitrate procedure (MGNP) using different precursors. By using the precursors such as metal acetates and glycine, one can control combustion and prepare nanosized oxides. The results show that applying MGNP method is possible to produce low price composition $Gd_{0.1}Ca_{0.9}MnO_3$ with particle size smaller than 20 nm and for relatively short time. Thus, this method proves to be adequate for the preparation of this particular composition. Although no large difference between used precursors exists, the best results were achieved by reaction (1), Section 2.

XRD pattern of $Gd_{0.1}Ca_{0.9}MnO_3$ sample showed that it crystallizes in the orthorhombic perovskite phase. As a result of doping $CaMnO_3$ with Gd, larger Mn^{3+} ions appeared in B sites of perovskite phase together with Mn^{4+} ions. Rietveld refinement showed that Gd^{3+} replaces Ca^{2+} in position A and also makes an impact on the position B by causing the valence change of a fraction of manganese ions from 4+ into 3+ in order to maintain electro negativity. Unit cell volume and average Mn–O bond distance analyses confirmed the results of Rietveld refinement. The obtained $Ca_{0.9}Gd_{0.1}MnO_3$ powders

are in nanometric range that is confirmed by calculations on the basis of XRD data.

Magnetic measurements show that doping by even small amount of Gd^{3+} ions substantially changes $CaMnO_3$ antiferromagnetic behaviour. After Gd^{3+} introduction, due to a double exchange interaction between Mn^{3+} and Mn^{4+} ions, significant ferromagnetic component appears. This is visible as a plateau in FC magnetization and a pronounced hysteresis loop, with relatively high coercivity ($H_C = 2000$ Oe) and remanence magnetization ($M_R = 2.95$ emu/g). Randomness and presence of competing AFM and FM interactions lead to a frustration of manganese magnetic moments so at low temperatures a spin-glass state appears. High temperature magnetic susceptibility obeys Curie–Weiss law from where effective magnetic moment of manganese $\mu_{eff} = 3.96\mu_B$ as well as Curie–Weiss temperature $\theta_P = (21.5 \pm 0.4)$ K are determined. Positive θ_P values, like in other similar systems, speaks in favour of the presence of FM clusters in antiferromagnetic matrix.

Acknowledgment

This project was financially supported by the Ministry of Science and Environmental Protection of Serbia (project number: 45012).

References

[1] J.M.D. Coey, M. Viret, S. Von Molnár, Mixed-valence manganites, Adv. Phys. 48 (1999) 167–293.
[2] A. Moreo, S. Yunoki, E. Dagotto, Phase separation scenario for manganese oxides and related materials, Science 283 (1999) 2034–2040.
[3] G.V. Subba, B.M. Wankyn, C.N.R. Rao, Electrical transport in rare earth ortho-chromites, -manganites and -ferrites, J. Phys. Chem. Solids 32 (1971) 345–358.
[4] R. Mahesh, R. Mahendiran, A.K. Raychauri, C.N.R. Rao, Effect of the internal pressure due to the A-site cations on the giant magnetoresistance and related properties of doped rare earth manganates, $Ln_{1-x}A_xMnO_3$ (Ln = La, Nd, Gd, Y; A = Ca, Sr, Ba, Pb), J. Solid State Chem. 120 (1995) 204–207.
[5] B. Dabrowski, P.W. Klamut, Z. Bukowski, R. Dybzinski, J.E. Siewenie, Effective oxygen content and properties of $La_{0.74}Ca_{0.26}MnO_{3+d}$ as a function of synthesis conditions, J. Solid State Chem. 144 (1999) 461–466.
[6] K. Cherif, J. Dhahri, E. Dahri, M. Oumezzine, H. Vincent, Effect of the A cation size on the structural, magnetic, and electrical properties of perovskites $(La_{1-x}Nd_x)_{0.7}Sr_{0.3r0.03n}MnO_3$, J. Solid State Chem. 163 (2002) 466–471.
[7] A. Asamitsu, Y. Tokura, Hall effect in $La_{1-x}Sr_xMnO_3$, Phys. Rev., B 58 (1998) 47–50.
[8] C.L. Bull, P.F. McMillan, Raman scattering study and electrical properties characterization of elpasolite perovskites $Ln_2(BB')O_6$ (Ln = La, Sm, ... Gd and B, B′ = Ni, Co, Mn), J. Solid State Chem. 177 (2004) 2323–2328.
[9] M. Muroi, R. Street, P.G. McCormick, Structural and magnetic properties of ultrafine $La_{0.7}Ca_{0.3}MnO_z$ powders prepared by mechanical alloying, J. Solid State Chem. 152 (2000) 503–510.
[10] M. Muroi, R. Street, P.G. McCormick, Enhancement of critical temperature in fine La...Ca...MnO... particles prepared by mechanochemical processing, J. Appl. Phys. 87 (2000) 3424–3431.
[11] P. Katiyar, D. Kumar, T.K. Nath, A.V. Kvit, J. Narayan, S. Chattopadhyay, W.M. Gilmore, S. Coleman, C.B. Lee, J. Sankar, R.K. Singh, Magnetic properties of self-assembled nanoscale $La_{2/3}Ca_{1/3}MnO_3$ particles in an alumina matrix, Appl. Phys. Lett. 79 (2001) 1327–1329.
[12] J. Dukić, S. Bošković, B. Matović, Crystal structure of Ce-doped $CaMnO_3$ perovskite, Ceram. Int. 35 (2009) 787–790.
[13] M. Mogensen, D. Lybye, N. Bonanos, P.V. Hendriksen, F.W. Poulsen, Factors controlling the oxide ion conductivity of fluorite and perovskite structured oxides, Solid State Ionics 174 (2004) 279–286.
[14] S. Hirano, J. Sugiyama, T. Noritake, T. Tani, Chemical pressure effect on magnetic properties in electron-doped perovskite manganites $(Gd_{0.08}Ca_ySr_{0.92-y})MnO_3$ ($0 < y < 1$): percolation transition of ferromagnetic clusters, Phys. Rev. B 70 (2004), 094419-1–094419-8.
[15] Y. Wang, Y. Sui, W. Su, High temperature thermoelectric characteristics of $Ca_{0.9}R_{0.1}MnO_3$ (R = La, Pr, ..., Yb), J. Appl. Phys. 104 (2008), 093703-1–093703-8.
[16] L. Sudheendra, A.R. Raju, C.N.R. Rao, A systematic study of four series of electron-doped rare earth manganates, $Ln_xCa_{1-x}MnO_3$ (Ln = La, Nd, Gd and Y) over the $x = 0.02$–0.25 composition range, J. Phys. Condens. Matter 15 (2003) 895–905.
[17] I. Medvedeva, A. Maignan, C. Martin, K. Bärner, B. Raveau, Yu. Bersenev, N. Mushnikov, E. Gerasimov, Hydrostatic pressure effect on electrical and magnetic properties of electron-doped $R_{0.16}Ca_{0.84}MnO_3$ (R = Pr, Gd, Eu), Physica B 365 (2005) 114–120.
[18] S.B. Bošković, B.Z. Matović, M.D. Vlajić, V.D. Kristić, Modified glycine nitrate procedure (MGNP) for the synthesis of SOFC nanopowders, Ceram. Int. 33 (2007) 89–93.
[19] K.C. Patil, M.S. Hegde, T. Rattan, S.T. Aruna, Chemistry Of Nanocrystalline Oxide Materials: Combustion Synthesis: Properties and Applications, World Scientific Publishing Co., Pte. Ltd., Singapore, 2008.
[20] S.R. Nair, R.D. Purohit, A.K. Tyagi, P.K. Sinha, B.P. Sharmaz, Low-temperature sintering of $La(Ca)CrO_3$ powder prepared through the combustion process, J. Am. Ceram. Soc. 91 (2008) 88–91.
[21] A. Kostić-Pulek, S. Marinković, R. Tomanec, M. Logar, The influence of magnesium chloride concentration in the liquid phase on the hydrothermal dehydration of gypsum, Ceram. Silik. 38 (1994) 173–177.
[22] J. Rodriguez-Carvajal, FullProf computer program, 1998, ftp://charybde.-saclay.cea.fr/pub/divers/fullprof.98/windows/winfp98.zip.
[23] J. Rodríguez-Carvajal, Recent advances in magnetic structure determination by neutron powder diffraction, Physica B 192 (1993) 55–69.
[24] J. Rodríguez-Carvajal, Recent developments of the program FULLPROF, in commission on powder diffraction (IUCr), Newsletter 26 (2001) 12 http://journals.iucr.org/iucr-top/comm/cpd/Newsletters/.
[25] C.H. Yan, Z.G. Xu, F.X. Xheng, Z.M. Wang, L.D. Sun, C.S. Liao, J.T. Jia, Nanophased $CoFe_2O_4$ prepared by combustion method, Solid State Commun. 111 (1999) 287–291.
[26] Y.-J. Yang, T.-L. Wen, H. Tu, D.-Q. Wang, J. Yang, Characteristics of lanthanum strontium chromite prepared by glycine nitrate process, Solid State Ionics 135 (2000) 475–479.
[27] B.D. Cullity, S.R. Stock, Elements of X-ray Diffraction, 3rd ed., Prentice-Hall Inc., 2001, pp. 167–171.
[28] Q. Zhou, B.J. Kennedy, Thermal expansion and structure of orthorhombic $CaMnO_3$, J. Phys. Chem. Solids 67 (2006) 1595–1598.
[29] E. Dagotto, J. Burgy, A. Moreo, Nanoscale phase separation in colossal magnetoresistance materials: lessons for the cuprates? Solid State Commun. 126 (2003) 9–22.
[30] D. Markovic, V. Kusigerski, M. Tadic, J. Blanusa, V. Antisari, V. Spasojevic, Magnetic properties of nanoparticle $La_{0.7}Ca_{0.3}MnO_3$ prepared by glycine-nitrate method without additional heat treatment, Scr. Mater. 59 (2008) 35–38.
[31] X.J. Fan, H. Koinuma, T. Hasegawa, Ferromagnetic correlation and metallic behavior in slightly electron-doped antiferromagnetic $CaMnO_3$, Physica B 329 (2003) 723–724.
[32] O. Peña, M. Bahout, K. Ghanimi, P. Duran, D. Gutierrez, C. Moure, Spin reversal and ferrimagnetism in (Gd, Ca)MnO_3, J. Math. Chem. 12 (2002) 2480–2485.
[33] J.A. Mydosh, Spin Glasses: An Experimental Introduction, Taylor and Francis, London, 1993.